



# Multifractal signal generation by cascaded chaotic systems and their analog electronic realization

Paweł Oświęcimka · Stanisław Drożdż ·  
Leonardo Ricci · Pedro A. Valdes-Sosa ·  
Mattia Frasca · Ludovico Minati

Received: 4 October 2023 / Accepted: 3 January 2024 / Published online: 12 February 2024  
© The Author(s), under exclusive licence to Springer Nature B.V. 2024

---

P. Oświęcimka · S. Drożdż  
Complex Systems Theory Department, Institute of Nuclear  
Physics, Polish Academy of Sciences, 31–342 Kraków, Poland

P. Oświęcimka  
Institute of Theoretical Physics and Mark Kac Center for Com-  
plex Systems Research, Jagiellonian University, 30-348 Kraków,  
Poland

S. Drożdż  
Faculty of Computer Science and Telecommunications, Cracow  
University of Technology, 31–155 Kraków, Poland

L. Ricci  
Department of Physics and Center for Mind/Brain Science  
(CIMEC), University of Trento, 38123 Trento, Italy

P. A. Valdes-Sosa  
School of Life Science and Technology, University of Electronic  
Science and Technology of China, 611731 Chengdu, China

Department of Neuroinformatics, Cuban Neuroscience Center,  
11600 Havana, Cuba

M. Frasca  
Department of Electrical Electronic and Computer Engineering,  
University of Catania, 95131 Catania, Italy

“A. Ruberti” Institute for Systems Analysis and Computer Sci-  
ence, National Research Council (IASI-CNR), Rome 00185,  
Italy

L. Minati (✉)  
School of Life Science and Technology, University of Electronic  
Science and Technology of China, 611731 Chengdu, China  
e-mail: lminati@uestc.edu.cn; ludovico.minati@unitn.it;  
lminati@ieee.org

L. Minati  
Center for Mind/Brain Science (CIMEC), University of Trento,  
38123 Trento, Italy

**Abstract** Multifractality, that is, self-similarity where in scaling follows a continuous spectrum of exponents, is a ubiquitous property of the morphology and dynamics of large-scale complex systems. However, to date, the prerequisites for the generation of multifractal time series by dynamical systems remain an open issue. This work demonstrates that multifractality can emerge in the time series spontaneously generated by a small ensemble of cascaded nonlinear oscillators, which are deterministic, autonomous and delayless. Namely, a chain of four Rössler systems with directed couplings is investigated numerically and realized experimentally in the form of analog electronic circuits. The observation of multifractality is established using the detrended fluctuation analysis and confirmed through surrogate tests, wavelet-based analyses and cascade structure visualization. Multifractality consistently arises when the oscillation frequencies of the coupled oscillators span a sufficient range along the chain, and the couplings have an intermediate strength which engenders partial entrainment between the adjacent nodes. These results affirm that neither external entropy injection nor driving are indispensable, and provide a blueprint for the design of self-contained generative circuits toward diverse applications across physiology modeling and unconventional computing.

**Keywords** Analog electronic circuits · Bifurcation cascade · Complexity · Multifractal spectrum · Multiscaling · Times series classification

## 1 Introduction

### 1.1 Background

Multifractal analyses have been widely used to characterize the scaling properties of time series across diverse scientific problems in physics [1–3], chemistry [4], neuroscience [5,6], economy [7–9] literature and art [10,11]. Determining the scaling exponents  $\alpha$  and thus forming a spectrum of singularities  $f(\alpha)$  provides a detailed description of the fractality of a time series, consequently offering profound insights into the physics of the underlying processes [12] and representing a primary basis for defining measures of complexity [13]. Since nonlinear dynamics are the fundamental source of multifractality, the scaling exponents contain information that is invisible to linear analyses based on the autocorrelation or power spectrum. The usefulness of multifractal analysis has led to the development of algorithms for directly estimating the singularity spectra of time series without requiring reconstructing the geometry of the underlying attractor [14–16]; these algorithms have subsequently been generalized to the assessment of cross-correlation [17]. At the same time, the pervasiveness of multifractality in nature has motivated considerable efforts toward understanding the conditions necessary for its generation and toward devising generative models. Currently, approaches based on multiplicative cascades, whereby multifractal time series are generated as a product of tree-like cascades with deterministic or stochastic parameters called multipliers, are prevalent [18,19]. An alternative to cascade-like processes with a discrete scaling ratio is a multifractal random walk that generates multifractal time series with stationary increments and a continuous invariance ratio [20].

In parallel with a growing appreciation of the importance of fundamental aspects of complexity such as multifractality, over the recent years, there has been a growing emphasis on investigating the universality of nonlinear dynamical phenomena, for example, concerning phase transitions and pattern formation via synchronization [21]. The interest in realizing electronic models of the most diverse dynamics found across physics, biology and other disciplines finds its roots in the early days of computing when analog circuits were widely used to integrate equation systems [22]. Unlike digital calculating machines, which directly embody numerical algorithms, analog electronic circuits are

continuous physical devices; the latter are also considerably more versatile than mechanical apparatuses and easier to realize and manipulate than optical setups [23]. Therefore, researchers from diverse fields have not only used circuit synthesis techniques to deploy analog computing by realizing equation systems as close as possible to verbatim. They have also, and especially, been trying to establish parallels between the behaviors of elementary analog electronic circuits, including nonlinearities such as multipliers, diodes and transistors, and the most diverse large-scale systems in physics, biology, social science and so on [24,25]. On the one hand, this is interesting from the perspective of investigating the universality of nonlinear dynamical phenomena. On the other hand, it is important from an applications perspective: as the limits of digital computing in terms of power efficiency and integration become evident, engineers are searching for new paradigms inspired by nature to address problems in signal generation, control and pattern analysis [26]. A notable example is the notion of physical reservoir computing, whereby elementary apparatuses, circuits and networks can be used to project an input vector to a higher-dimensional representation where linear separability is possible [27].

### 1.2 Multifractality in electronic circuits

Through a multitude of different analog circuits, often endowed with a certain level of structural elegance, fundamental dynamical phenomena such as low- and high-dimensional chaos, quasiperiodicity, criticality, first- and second-order phase transitions have been extensively demonstrated [25,28,29]. Intriguingly, despite its pervasiveness in nature, the literature is considerably more sparse as regards electronic generators of multifractality. Multifractal scaling has been reported as an emergent property in the dynamics of telecommunication networks, power distribution networks and in CMOS circuits subject to random excitation; however, there are almost no examples of elementary circuits that generate multifractal time series by design [30–32]. The notion of multifractality is intimately linked to that of turbulence, and accordingly, its observation is almost invariably associated with dynamics that possess a stochastic component [33,34]. However, to the authors' knowledge, it is not possible to rigorously assert that noise is a fundamental prerequisite for it:

on the contrary, the analytical properties of the binomial cascade and the generation of multifractal geometries by iterated maps point in the opposite direction [35]. Nevertheless, one prevailing perspective on multifractality has been that of random multiplicative processes, whereby the influence of noise unfolds over time depending on the evolution of a system's state. This notion has proven highly relevant to understanding, for example, the dynamics of fluids and agents in noisy environments [36,37].

From an electronic viewpoint, the coexistence of multiple sources of differently colored noise is well established, dominated but not limited to thermal noise. Leveraging these generators, realized, for example, using a resistor or diode, noise source circuits are readily obtainable, and can be easily combined with an additional stage providing the multiplicative effect, yielding power law effects [38,39]. Using this approach, the possibility of generating a multifractal time series using just two operational amplifiers was shown; however, this remains an isolated observation [40]. This paucity of multifractal signal-generating circuits in the literature is surprising also given that early papers on the  $f(\alpha)$  formalism demonstrated broad spectra close to of chaotic transitions, in the attractor geometries generated by circuits such as driven diode-resonator systems and other apparatuses. However, as discussed below, a crucial limitation is that those studies did not address the multifractality of the time series as such, as is customarily done today to investigate it in the context of large-scale complex systems [28,41,42]. Furthermore, recent work has highlighted the potential of multifractality as a generative mechanism in optical and optoelectronic systems [43].

### 1.3 Purpose

Ultimately, whether multifractal time series could be generated by a dynamical system that is fully deterministic, that is, wherein noise does not play a fundamental generative role, and, consequently, by its electronic circuit realization, essentially remains an open question. The distinction is important since, effectively, circuits that fundamentally require an external noise source do not correspond to autonomous dynamics and are therefore considered not self-contained, thus less fundamental and desirable, and more vulnerable to external attacks [44]. Throughout previous

attempts omitted for brevity, the authors had extensively searched for signatures of multifractal time series in the dynamics of individual low-dimensional chaotic, high-dimensional chaotic and hyperchaotic analog electronic circuits, without finding any convincing evidence. In this paper, the first successful and consistent observation based on a fully deterministic and autonomous ensemble of dynamical systems is presented. The arrangement is elementary and consists of a cascade of four Rössler systems, which are studied both numerically and through experimental recordings from the corresponding circuit realization.

## 2 Detrended fluctuation analysis

To date, the fractal properties of a time series are usually characterized through the well-established multifractal detrended fluctuation analysis (MFDFA) [15]. According to this approach, the self-similarity of a signal is quantified by a set of exponents representing the scaling properties of the fluctuations with respect to their amplitudes. The usefulness of this method has led to its widespread use in describing signal complexity across various fields of research [45,46]. The MFDFA comprises several steps, which are described in detail below and can be summarized as follows:

- Step 1: Obtain the integrated time series through subtracting the mean and calculating the cumulative sum;
- Step 2: Divide such time series into  $N_s$  non-overlapping segments of identical length  $s$ ;
- Step 3: Calculate and remove the local trend for each segment;
- Step 4: Gather the averaged local variances into the  $q$ th-order fluctuation functions. Repeat this operation for each time scale  $s$ ;
- Step 5: Determine the multifractal properties of the time series by estimation slope coefficients  $h(q)$  of the fluctuation functions;
- Step 6: Calculate the multifractal spectrum  $f(\alpha)$ , its width  $\Delta\alpha$  and asymmetry  $A_\alpha$ .

A comprehensive and accessible tutorial on MFDFA can be found in Ref. [47].

More in detail, as Step 1, the profile, or mean-subtracted cumulative sum,  $U(j)$  of a sample vector  $u_i$  having length  $N$ , is calculated as

$$U(j) = \sum_{i=1}^j [u_i - \langle u \rangle], \quad (1)$$

where  $j = 1, 2, \dots, N$  and  $\langle x \rangle$  denotes the average value. The presence of self-similar patterns, alias the fractality, of the time series is quantified by analyzing the signal statistical properties over diverse temporal scales. To this end, as Step 2, the time series is subdivided twice into  $2N_s$  non-overlapping segments of length  $s$ , where  $N_s = \lfloor N/s \rfloor$ , once starting from the beginning and once starting from the end of the time series. This procedure ensures that none of the data points are missed by the analysis. To attenuate possible nonstationarity, as Step 3, a polynomial of order  $m$  is fitted to each segment, identified with an index  $v = 1, 2, \dots, N_s$  and obtained in this way, and then subtracted from the data. To remove possible trends from the data adequately while preserving the fluctuation structure, the polynomial order has to be relatively low. Throughout this paper, we assume  $m = 2$ , but this setting is not critical.

Subsequently, as Step 4, the detrended variances are calculated over all the segments  $v$  according to

$$F^2(v, s) = \frac{1}{s} \sum_{k=1}^s U((v-1)s+k) - P_v^{(m)}(k))^2, \quad (2)$$

where  $P_v^{(m)}$  denotes the fitted polynomial of order  $m$  in the segment of index  $v$ . To assess the multifractal properties of the signal, the fluctuation function is thereafter calculated with

$$F_q(s) = \left\{ \frac{1}{2N_s} \sum_{v=1}^{2N_s} [F^2(v, s)]^{q/2} \right\}^{1/q}, \quad q \in \mathfrak{R} \setminus \{0\}. \quad (3)$$

As Step 5, the usage of the  $q$  exponent in Eq. (3) reflects the application of the  $q$ -filtering technique, through which the scaling properties of the fluctuations can be quantified as a function of their amplitude. Specifically, small  $q$  values enhance the influence of minor fluctuations, whereas large  $q$  values amplify the major ones. For fractal time series, the power law-like behavior of the fluctuation function holds over a large span of scales, with

$$F_q(s) \sim s^{h(q)}, \quad (4)$$

where  $h(q)$  is the generalized Hurst exponent. This relation can be depicted in a double logarithmic plot

representation as a linear one having slope coefficients  $h(q)$ , which can be estimated by the least squares method. In particular, for monofractals,  $h(q)$  is independent of  $q$  and equals the Hurst exponent  $H$ , whereas, for multifractals,  $h(q)$  is a decreasing function of  $q$  (with  $h(2) = H$ ). The Hurst exponent quantifies the linear interdependencies between time points: for  $H > 0.5$ , the signal features positive autocorrelation (persistence), whereas, for  $H < 0.5$ , negative dependencies are preferentially observed (antipersistence). For  $H = 0.5$ , there is no consistent linear relationship between adjacent samples in the signal. To visualize the spectrum of the scaling exponents and the difference between the monofractal and multifractal structure,  $h(q)$  is transformed into a multifractal spectrum using

$$\alpha = h(q) + qh'(q), \quad f(\alpha) = q[\alpha - h(q)] + 1, \quad (5)$$

where  $\alpha$  is the Hölder exponent, and  $f(\alpha)$  denotes the fractal dimension of the data supported by a particular  $\alpha$ .

Finally, as Step 6, the strength of multifractality is finally quantified in terms of the width of the multifractal spectrum,

$$\Delta\alpha = \alpha_{\max} - \alpha_{\min}; \quad (6)$$

the broader the spectrum (larger  $\Delta\alpha$ ), the more developed the multifractality. Another feature of the multifractal spectrum is its asymmetry, which reflects other aspects of the temporal organization of the data. For the artificially generated deterministic binomial cascade spectrum,  $f(\alpha)$  is symmetric, indicating a balanced organization of large and small fluctuations. However, for real-world signals the spectrum is often asymmetric, indicating a more developed correlation structure for large fluctuations (left-sided asymmetry) or small ones (right-sided asymmetry). The asymmetry parameter is defined as

$$A_\alpha = (\Delta\alpha_L - \Delta\alpha_R) / (\Delta\alpha_L + \Delta\alpha_R), \quad (7)$$

where  $\Delta\alpha_L = \alpha^{(\max)} - \alpha_{\min}$  and  $\Delta\alpha_R = \alpha_{\max} - \alpha^{(\max)}$ , with  $f(\alpha^{(\max)}) = \max[f(\alpha)]$  [48]. According to this definition, positive and negative values of  $A_\alpha$  denote, respectively, leftwards- and rightwards-stretched spectra.

In keeping with previous work searching for multifractality in the time series generated by oscillator circuits, we generated two kinds of surrogates to confirm the statistical reliability of the results [16]. The

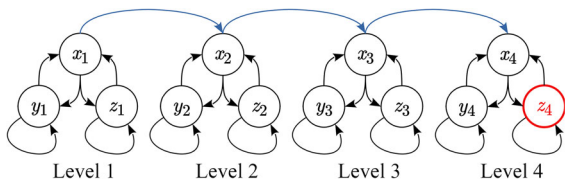


**Fig. 1** Fluence diagram of Eq. (8). Blue: Inter-level couplings. Red: Preferential variable for multifractality observation (see text)

first set was obtained by randomly shuffling the original time series, thus destroying the temporal organization of the data. The second set was obtained by randomly shuffling the phases of the Fourier transform of the signal while preserving the amplitudes [49]. Consequently, the linear autocorrelation structure, reflected in the Fourier amplitudes, remains unchanged, but all the nonlinear properties are destroyed. In both cases, the multifractal spectrum is expected to collapse into a point, located, respectively, either around  $\alpha = 0.5$  or overlapping the spectrum of the original data.

### 3 Simulations

#### 3.1 System definition

As depicted in Fig. 1, throughout the paper, we consider the Rössler system as node dynamics and realize a chain of four nodes coupled unidirectionally, referred to as levels 1–4. This selection of node dynamics was made not only in virtue of the fact that the Rössler system is considered a canonical example of low-dimensional chaos but also because it is considerably less prone to undergoing orbit ejection when driven by an arbitrary external signal compared to the alternatives [50–54]. For example, the Lorenz system is similarly three-dimensional and well-studied; however, it features double-scroll dynamics and the topology of the underlying attractor is accordingly profoundly different. While there is no strong theoretical motivation for choosing the Rössler system over the Lorenz system for this work, in preliminary investigations the Rössler system was found to be more robust to divergence (orbit ejection) in the present configuration. No less importantly, the electronic realization of the Lorenz system is more complex, as it requires two instead of one analog multiplier. At the same time, Chua's circuit and the jerk circuit represent equally suitable low-

dimensional system alternatives; however, their nonlinearity is more complex from a mathematical point of view, consisting, respectively, of an exponential term and a piece-wise nonlinearity, instead of a product [55]. High-dimensional chaos generators, such as those based on fractal resonators, would also be worth considering; however, in earlier works, they were not found to generate multifractal signatures, and are considerably more complex, structurally and electronically [56]. A systematic investigation of other chaotic systems in the context of the present arrangement is acknowledged to be necessary and left for others to pursue.

The idea of cascading chaotic systems has already been explored in other areas for the purpose of obtaining high-dimensional signals [57]. A brief reflection on the advantages and disadvantages of this approach is motivated. The primary advantage is that cascading is, in principle, agnostic to the specific dynamical system instantiated at each level and, therefore, generalizable. Furthermore, it inherently enjoys some conceptual affinity to the concept of binomial cascade, which is a mathematical model of a multifractal [58,59]. The obvious disadvantage is the lack of compactness, in that observing multifractality in an individual dynamical system would be more compelling, and more conducive toward understanding the underlying mechanisms.

Here, the arrangement as a cascade was realized through four choices. First, each node provides energy to the next one through a unidirectional coupling, in the direction from the slower to the faster dynamics, as elaborated below. A reason for this choice is that, since the Rössler system includes a low-pass frequency filtering effect, a slower node could effectively disturb a faster one, but external signals at frequencies higher than the intrinsic dynamics are attenuated. This may be observed and considering the transfer function from an external input  $i(t)$  to variable  $y(t)$  assuming  $z = 0$ , which reads  $\text{TF}(s) = k\omega_i^2 / (s^2 + \omega_i^2)$  and thus has a complex conjugate pole at  $\omega_i$ , and considering the RC integrators instantiated in the electronic circuit described in the next Section. Another reason is conceptual, namely that the notion of a cascade fundamentally entails the coarser scales influencing the finer ones, and not vice versa [58,59]. Finally, during initial evaluation omitted for brevity, replacing unidirectional with bidirectional coupling was confirmed to have a negligible effect on the emergence of multifractality; therefore, the most parsimonious configuration was retained.

Second, the couplings are realized through an additional forcing-like term  $+ki(t)$ , such that the energy exchange rate is independent of the mismatch, as normally associated with the periodic forcing terms found in non-autonomous systems [60]. From a physical perspective, this form of coupling is different from the diffusive mechanisms realized, for example, using springs and resistors, and akin to mechanisms such as optical pumping and synapses, where the amount of photons entering a cavity or neurotransmitter released toward a dendrite is independent of its current state [21]. Conceptually, this is also in line with the fact that in a cascade, each level influences the ones below in a way that is not determined by their state [58,59]. Preliminary analyses, omitted for brevity, indicated that multifractality emerged with coupling terms of the form  $+ki(t)$  and not  $+k[i(t) - x(t)]$ ; therefore, this choice was retained.

Third, the coupling is realized on the  $x$  variable. While the effect of the coupling variable(s) on synchronizability can in certain cases be determined using the master stability function, in this case, the coupling mechanisms and strong frequency mismatch hinder the application of this approach [61]. During initial experiments with the present arrangement, coupling using the variable  $x$  was found to be considerably more robust to divergence compared to using the  $y$  variable; the former variable is also the one most frequently selected for coupling in the chaos synchronization literature [62]. The answer can be found considering the fluence graph of the system alongside its transfer functions. The variable  $z$  on which the nonlinearity acts both draws from and influences the  $x$  variable. The transfer function from the input to the variable to which it is structurally coupled has a zero at the origin, which has a differentiating effect. Therefore, if the input is coupled to the  $x$  variable, it is differentiated before being integrated, whereas, if it is coupled to  $y$ , the converse is true, promoting the emergence of large swings in  $x$  and, in turn, divergence [52]. On the other hand, given the jerky nature of its motion, the  $z$  variable itself was not considered for coupling.

Four, the time scales of the dynamics across the coupled nodes, regulated by the parameters  $\omega^{k_i}$ , follow a geometric sequence in the powers  $k_i$  with base value 2, so that, for  $i > 1$ , the ratio  $k_{i+1}/k_i = 2$  remains constant for each pair of cascaded oscillators, whereby the slower nodes drive the faster ones. In other words,  $\omega_1 = 1$ ,  $\omega_2 = \omega$ ,  $\omega_3 = \omega^2$  and  $\omega_4 = \omega^4$ . In a binomial

cascade, a level divides each subinterval of the previous one into 2, whereas, in these oscillators, each level  $i$  divides the characteristic period of the previous one by a power of  $\omega$  in geometric progression. The role of the time scale  $\omega$ , therefore, is to steeply determine the separation between levels. For  $\omega = 1$ , there is no separation, namely  $\omega_1 = \omega_2 = \omega_3 = \omega_4$ . On the other hand, considering the typical setting  $\omega = 2.5$  reported below, the frequency ratio between the fastest and the slowest dynamics is  $\omega^4/\omega^0 = 39$ . Adding a fifth level would have resulted in  $\omega^8/\omega^0 = 1526$ ; since, as shown below, four levels were sufficient for observing multifractality, and adding a fifth one would have caused a prohibitive computational load in the simulations due to its influence on the solver step size and practical issues related to frequency span and recording length in the experiments, the cascade was truncated at four levels. The investigation of deeper cascades and different scaling progressions is left for future work.

The resulting 12-dimensional system,

$$\begin{cases} \frac{dx_1}{dt} = -y_1 - z_1 \\ \frac{dy_1}{dt} = x_1 + ay_1 \\ \frac{dz_1}{dt} = b + (x_1 - c)z_1 \\ \frac{dx_2}{dt} = \omega(-y_2 - z_2 + kx_1) \\ \frac{dy_2}{dt} = \omega(x_2 + ay_2) \\ \frac{dz_2}{dt} = \omega[b + (x_2 - c)z_2] \\ \frac{dx_3}{dt} = \omega^2(-y_3 - z_3 + kx_2) \\ \frac{dy_3}{dt} = \omega^2(x_3 + ay_3), \\ \frac{dz_3}{dt} = \omega^2[b + (x_3 - c)z_3] \\ \frac{dx_4}{dt} = \omega^4(-y_4 - z_4 + kx_3) \\ \frac{dy_4}{dt} = \omega^4(x_4 + ay_4) \\ \frac{dz_4}{dt} = \omega^4[b + (x_4 - c)z_4] \end{cases} \quad (8)$$

has three control parameters which were tuned in the below analyses: the bifurcation parameter  $a$  as defined in the Rössler system, varied globally over the four levels, the coupling coefficient  $k$  controlling the energy exchange between the nodes, and the rate  $\omega$ , controlling the degree of temporal separation across the levels. The other parameters of the Rössler system were fixed to  $b = 0.2$  and  $c = 5.7$ , representing a well-studied con-

figuration for this system [53,54]. For these settings, the Rössler system undergoes a bifurcation cascade for increasing  $a$ , and a greater coupling strength  $k$  is necessary to attain a given level of synchronization as the value of  $a$  is increased [21,50,51]. Unless otherwise noted, we focus on the case  $a = 0.15$ , approximately corresponding to the beginning of the bifurcation cascade (i.e., period 4 limit cycle), where the dynamics are maximally responsive to external influences. The temporal separation determined by  $\omega$  has a similar effect on the coupling strength needed to attain synchronization. For parsimony, the coupling strength  $k$  was set homogeneously across  $x_i \rightarrow x_{i+1}$ . The system was integrated with adaptive step size using the explicit Runge–Kutta Prince–Dormand order 4,5 formula until  $t_{\max} = 250 \times 10^3$  [63]. The initial conditions were randomly set in  $x \in [6, 8]$ ,  $y = z = 0$ ; as these values are in the vicinity of those assumed by the system variables crossing the  $(y, z)$  plane, the initial transient is kept relatively short [53,54]. Analogous results, not shown for brevity, were obtained using other suitable solvers.

### 3.2 Multifractal properties of the time series

To apply the multifractal detrended fluctuation analysis, the  $q$  moments as per Eq. (3) were considered over the range  $[-4, 4]$  with a step of 0.1 and excluding zero [64]. Throughout the paper, unless noted otherwise,  $12 \times 12$  bidimensional sweeps over the coupling strength  $k \in [0.09, 1]$  and frequency  $\omega \in [1.82, 5]$  were performed, and multifractal spectra were obtained for all the time series derived from the  $x$ ,  $y$  and  $z$  variables. An issue with the Rössler system and similar chaos generators is that their trajectories possess strong temporal autocorrelation, unlike the activity of large-scale complex systems such as financial time series [50–52]. To address this common situation in nonlinear time series analysis, the local maxima were identified using the first and second derivatives [65].

The qualitative features of the dynamics of the cascaded systems could be initially appreciated considering representative parameter settings, namely  $k = 0.7$  and  $\omega = 2.5$ . As shown in Fig. 2, by construction, given the unidirectional couplings, the dynamics of the first system in the cascade coincided with the known periodic behavior of a Rössler system for these settings. Already the second system displayed consider-

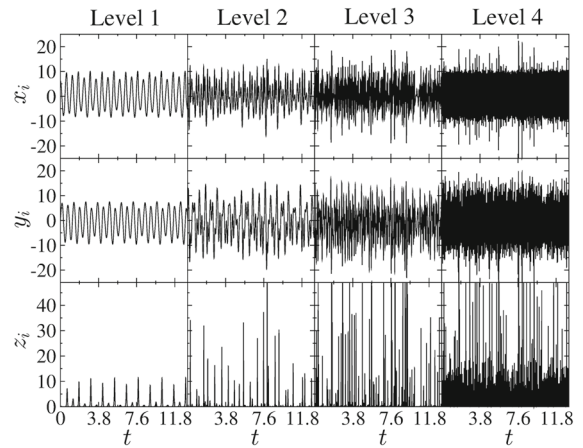


**Fig. 2** Time series obtained integrating the variables  $x$ ,  $y$  and  $z$  in Eq. (8), given  $\omega = 2.5$  and  $k = 0.7$

able irregularity, which became gradually more pronounced down along the chain, accompanied by a marked increase in the span of values visited by the  $z_i$  variables. As depicted in Fig. 3, a period 4 closed orbit was well evident at the first level, whereas, further down the chain, the corresponding area of the phase space became gradually more densely filled. The overall shape of the attractor appeared increasingly distorted compared to the original one, becoming devoid of the funnel-like profile and characterized by large excursions particularly for the  $z$  variable. The corresponding cumulative sums, visible in Fig. 4, were characterized by a gradual increase in volatility and fluctuation amplitude: the transition from the first to the second level featured a qualitative change from regular to highly irregular profiles, while, further down the chain, one could appreciate the establishment of irregular fluctuations over a broader range of scales, particularly visible through the appearance of large jumps.

Representative characteristics obtained for the  $z_4$  variable and two sets of system parameters, namely,  $\omega = 2.45$  and  $k = 0.63$ , and  $\omega = 2.14$  and  $k = 0.09$  are depicted in Fig. 5. The properties of the signals showed a marked, easily appreciable difference. For the first set, the analyzed signal revealed a clear multifractal organization, manifest through the family of power-laws governing the behavior of the fluctuation functions  $F_q(s)$ , visible in the form of a broad distribution of well-differentiated slopes of  $F_q(s)$  vs.  $s$  as a function of  $q$  in Fig. 5a. By contrast, for the second set, the signal showed at most monofractal features, as

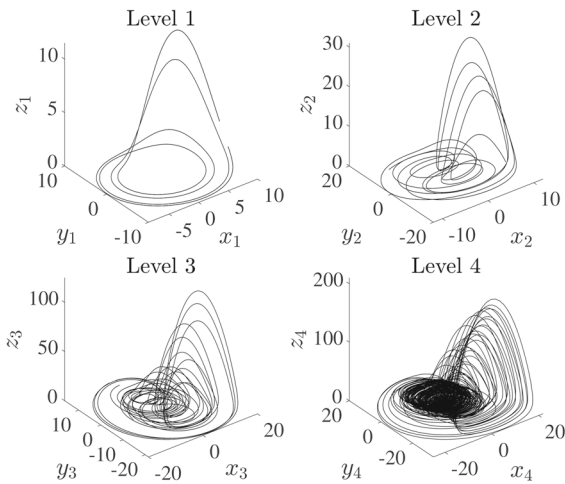


**Fig. 3** The attractors of the four cascaded systems, obtained integrating Eq. (8) with  $\omega = 2.5$  and  $k = 0.7$

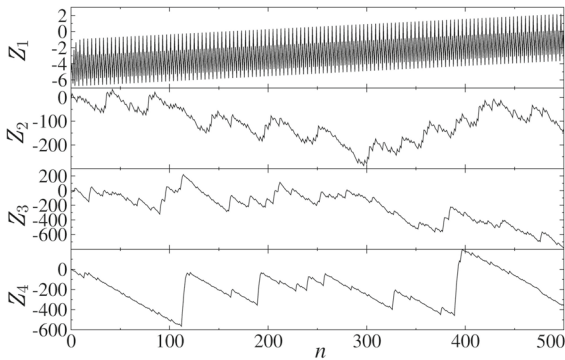


**Fig. 4** Cumulative mean-subtracted sums  $Z_i$  for the series of local maxima of the  $z_i$  time series, obtained integrating Eq. (8) with  $\omega = 2.5$  and  $k = 0.7$

depicted in Fig. 5b by the fact that the dependence of  $F_q(s)$  on  $s$  was largely insensitive to  $q$  and, accordingly, the fluctuation functions largely overlapped.

As regards the multifractal spectrum, the first case resulted in a large width,  $\Delta\alpha = 0.64$ , notable especially when compared to surrogate data  $\Delta\alpha = 0.02$ , and a characteristic shape of the distribution of  $f(\alpha)$  vs.  $\alpha$  resembling an inverted parabola, clearly confirming the multifractality. Moreover, the high symmetry of the spectrum  $A_\alpha = 0.03$  indicated a near-perfect balance between correlations of fluctuations of different amplitudes, closely resembling the known properties of the multifractal cascades [18–20]. By contrast, for the second set, the signal showed at most monofractal features, as depicted in Fig. 5b, with weak scaling of the fluctuation functions and, consequently, narrow multifractal

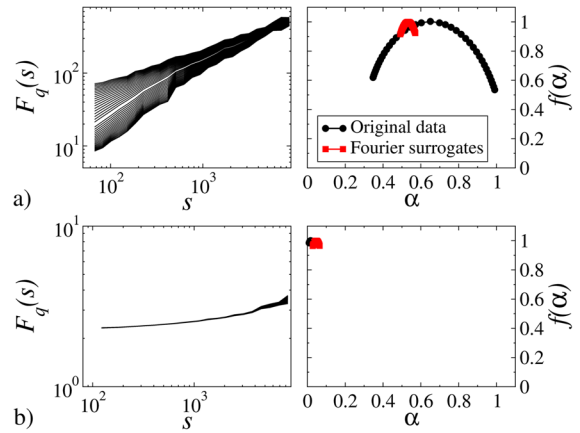


**Fig. 5** Sample fluctuation functions  $F_q(s)$  and multifractal spectrum  $f(\alpha)$  obtained for time series of variable  $z_4$  generated integrating Eq. (8) with **a**  $\omega = 2.45$ ,  $k = 0.63$  (corresponding to multifractality), **b**  $\omega = 2.14$ ,  $k = 0.09$  (corresponding to monofractality)

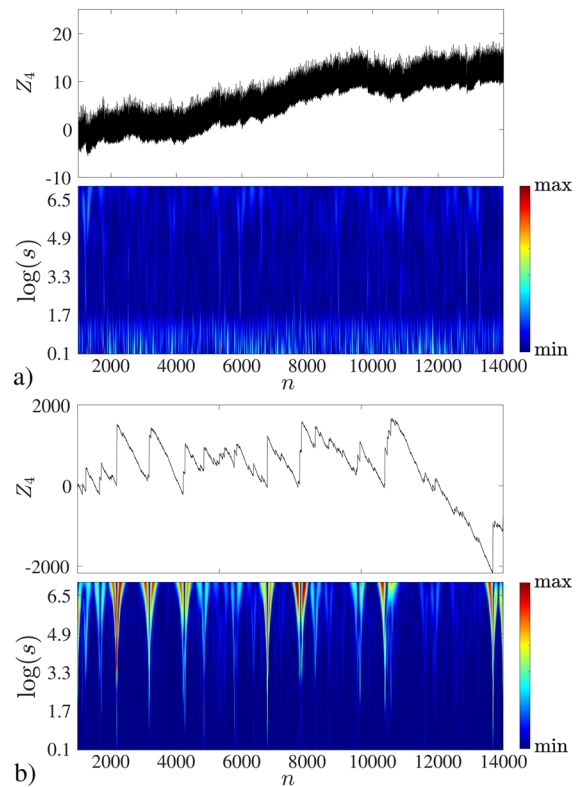


**Fig. 6** Wavelet transform of the  $z_4$  variable signal, obtained integrating Eq. (8) for  $\omega = 2.77$  and **a**  $k = 0.09$  (corresponding to monofractality), **b**  $k = 0.73$  (corresponding to multifractality)

spectra ( $\Delta\alpha = 0.03$ ), essentially collapsed down to a point indistinguishable from the surrogates. For  $z_1$  and  $z_2$ , multifractality was absent and, for  $z_3$ , it was weak, therefore, in the interest of brevity, throughout the rest of the paper, we consider directly  $z_4$ . A detailed analysis of the implications of the number of levels and type of scaling sequence is left for future work.

A further indication of the validity of multifractality was provided through the analysis of the local wavelet transform coefficients, conducted through the methods detailed in Ref. [16]. As depicted in Fig. 6a, for parameter settings associated with monofractality, the cumulative sum time series featured limited volatility. This was reflected in a relatively homogeneous distribution of the wavelet coefficients, devoid of large-scale regularity, that is, without hierarchical structure across the scales. By contrast, as shown in Fig. 6b, in the presence of multifractality, the cumulative sum series featured a markedly stronger volatility. Of fundamental importance, the wavelet coefficients enjoyed a well-formed tree-like organization, which was evident on the distribution of the same as a function of  $n$  and  $\log(s)$ , and stemmed from the self-similar organization of the fluctuations. If multifractality had been artificial, as previously reported, isolated singularities would have reflected into separate lines on the space-scale half-plane [16].

A more systematic view of the system’s multifractal organization was provided through the parameter sweeps in Fig. 7a, visualizing the width  $\Delta\alpha$ . It could be readily appreciated that the evolution of the local maxima belonging to the  $x_4$  and  $y_4$  variables was characterized by simple dynamics, with monofractal organization at most, and this observation was essentially independent of the settings of the control parameters  $k$  and  $\omega$ . In stark contrast, for the  $z$  variable, the multifractality was manifest as broad spectra delineating a kind of “complexity path” on the heatmap. Along this path, corresponding to intermediate combinations of coupling strength and frequency scaling, the spectral width reached  $\Delta\alpha \approx 0.6$  (reduced down to  $\Delta\alpha \approx 0.1$  for the surrogates), confirming an evident influence of the control parameters on the multifractal organization of the generated time series.

Closer inspection of the statistical properties of the  $x_4$ ,  $y_4$  and  $z_4$  variables revealed in more detail the manifold differences that developed among them at the last level of the cascade. The corresponding probability density functions, shown in Fig. 8 after normaliza-

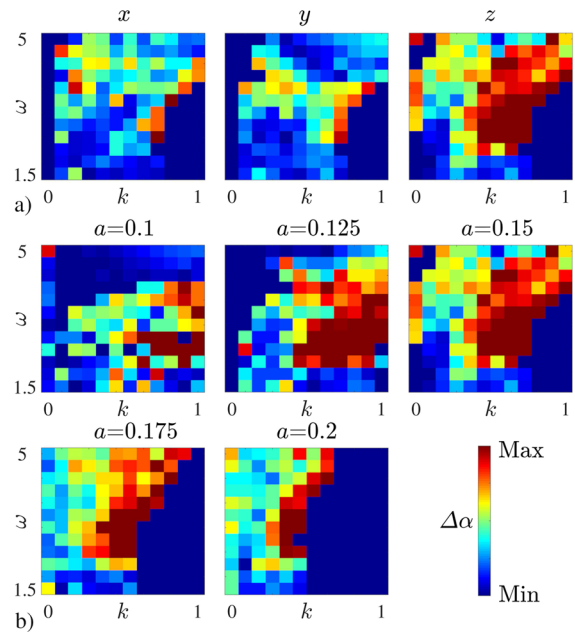


**Fig. 7** Parametric maps of  $\Delta\alpha$  as a function of  $k$  and  $\omega$  obtained integrating Eq. (8). **a** Comparison of the variables  $x_4$ ,  $y_4$  and  $z_4$ , given  $a = 0.15$ . **b** Effect of the bifurcation parameter  $a$ , visualized for the variable  $z_4$

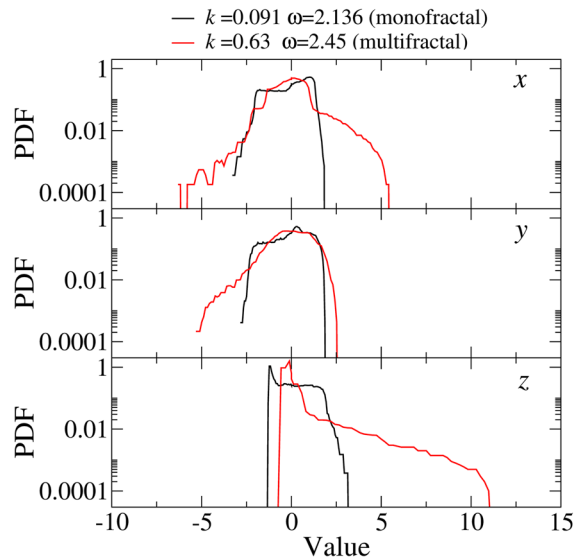


**Fig. 8** Probability distribution functions (PDFs) for the time series of the  $x_4$ ,  $y_4$  and  $z_4$  variables generated integrating Eq. (8). Median filter smoothing applied

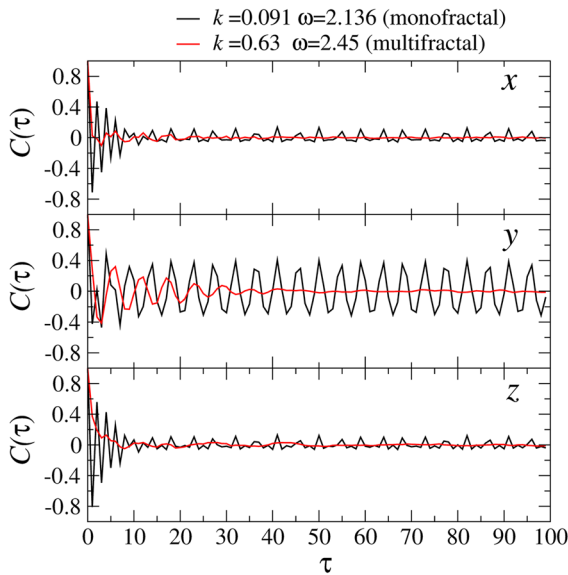


**Fig. 9** Auto-correlation functions  $C(\tau)$  for the time series of the  $x_4$ ,  $y_4$  and  $z_4$  variables generated integrating Eq. (8)

tion, demonstrated that, for parameter settings associated with monofractal dynamics, the distributions of all variables were compact and approximately symmetric. By contrast, for the multifractal case, the distribution of  $z_4$  appeared distinctly different than its counterparts for the other variables. Namely, its probability density function possessed a long exponential tail, illuminating a significant prevalence of large fluctuations in the signal, whereas the distribution tails of the other variables decayed considerably faster. Major differences were also visible in the corresponding autocorrelation functions, charted in Fig. 9. Namely, the autocorrelation function of  $z_4$  decreased monotonically toward zero, whereas for the other variables, it fluctuated around zero. The effects are plausibly related to the known differences in the qualitative aspects of the dynamics of the variables of the Rössler system, which in turn stem from the fact that the nonlinearity acts on the governing equation of the  $z$  variable.

To assess the system's sensitivity to the bifurcation parameter  $a$ , we performed addition calculations sweeping  $a \in [0.1, 0.2]$ , assessing the width of  $f(\alpha)$  as illustrated in Fig. 7b. Since compelling multifractality was identified for the  $z_4$  variable, we focused on this variable. It can be seen that the multifractality was strongly dependent on the setting of the bifurcation parameter  $a$ , in that well-developed spectra ensued

for  $a = \{0.125, 0.15\}$ , corresponding to the beginning of the bifurcation cascade (i.e., respectively, period 2 and period 4), whereas, for smaller and larger settings, monofractal behavior or lack of fractality prevailed. These observations were validated by surrogate data, not shown for brevity.

### 3.3 Relation to hyperchaos and synchronization

To investigate a possible relationship between multifractality and hyperchaos, the Lyapunov exponents were estimated via the “standard method”, which relies on evaluating orthogonal deviation vectors computed from the Jacobian matrix via Gram-Schmidt orthonormalization [66,67]. While solving the system in Eq. (8) assuming  $a = 0.15$ , all terms of the corresponding Jacobian matrix were also integrated, allowing estimating the entire spectrum of Lyapunov exponents. For this analysis, the integration was carried out over  $10^7$  steps via the explicit embedded Runge–Kutta Prince–Dormand order 8,9 method using a fixed step size of  $dt = 0.0025/\omega^4$ , considerably less than the typical time scale of the system's evolution resulting from a given value of the  $\omega$  parameter. The orthonormalization was set to take place every 80 steps. As shown in Fig. 10, the distributions of the Lyapunov exponents  $\lambda_i$  and consequently of the Kaplan–Yorke dimension  $D_{KY}$  were evidently uncorrelated to  $\Delta\alpha$ . The first three largest Lyapunov exponents tended to be positive everywhere; in other words, there was no correlation between the positiveness of the exponents and the presence of well-developed multifractality. The region where multifractality emerged was, instead, associated with intermediate values of these exponents and of the corresponding dimension which were, instead, maximized for strong couplings, thus refuting the hypothesized association.

In the presence of sufficiently intense coupling, structurally identical chaotic systems undergo phase synchronization at a unitary frequency ratio [21]. However, in Eq. (8), the coupled systems are by construction strongly mismatched due to the frequency scaling factors. This offered the opportunity to examine the possible locking between them assuming either a unitary ratio, or a ratio reflecting their characteristic frequencies. As the coupling coefficient is gradually increased, one expects that the frequencies of the coupled systems may be brought closer, shifting away from the  $n:m$  ratio directly determined by the  $\omega^k$  coefficients and toward

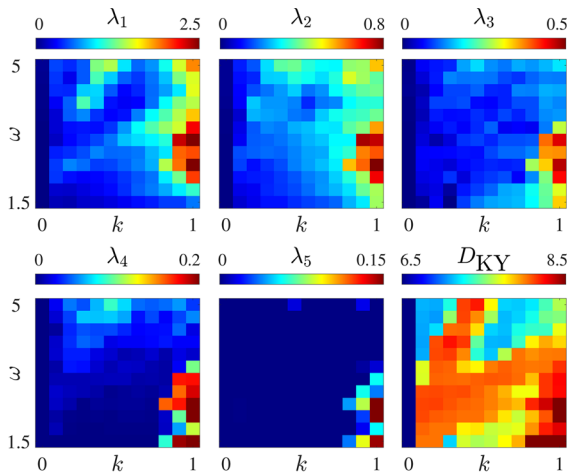


**Fig. 10** Parametric maps of the five largest Lyapunov exponents  $\lambda_i$  and Kaplan–Yorke dimension  $D_{KY}$  as a function of  $k$  and  $\omega$ , generated integrating Eq. (8)

the 1:1 ratio supported by energy exchange through the couplings. To examine this possibility, as detailed in Refs. [68,69] the analytic signals corresponding to the  $x_i$  variables were calculated according to

$$\psi_i(t) = x_i(t) + j\tilde{x}_i(t) = a_i(t)e^{j\theta_i(t)}, \tag{9}$$

where  $i = 1, 2 \dots 4$ ,  $j = \sqrt{-1}$ , and  $\tilde{u}(t)$  denotes the Hilbert transform of  $u(t)$ , namely,

$$\tilde{u}(t) = \frac{1}{\pi} \text{p.v.} \left[ \int_{-\infty}^{\infty} \frac{u(\tau)}{t - \tau} d\tau \right], \tag{10}$$

with p.v. signifying the Cauchy principal value of the integral, and the instantaneous phases were obtained with

$$\theta_i(t) = \arg [\psi_i(t)]. \tag{11}$$

The 1:1 and  $n:m$  phase synchronization values between the nodes  $i$  and  $i + 1$  could then be written, respectively, as

$$r_{i,i+1} = |\langle e^{j(\theta_i - \theta_{i+1})} \rangle_t|, \tag{12}$$

and

$$\tilde{r}_{i,i+1} = |\langle e^{j(\theta_i/\omega_i - \theta_{i+1}/\omega_{i+1})} \rangle_t|, \tag{13}$$

where, as previously indicated,  $\omega_i \in \{0, 1, 2, 4\}$  [70]. The corresponding parametric maps of phase synchronization are shown in Fig. 11. It can be seen that, for the 1 : 1 ratio, the level of entrainment gradually decreased with  $\omega$  and increased with  $k$ , in line

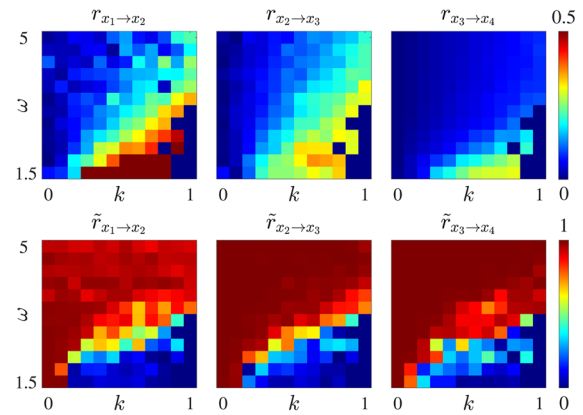


**Fig. 11** Parametric maps of the phase synchronization according to 1:1 and  $n:m$  ratios (i.e., given by the couplings vs. the predetermined  $\omega$  values), generated integrating Eq. (8)

with the expectation that stronger coupling is necessary to overcome a larger mismatch between the levels. A large region of imperfect phase synchronization, with  $r \approx 0.3$ , was observed at intermediate settings of these parameters. By contrast, the parametric maps for the  $n : m$  ratio featured an almost inverse distribution. For low levels of the coupling strength  $k$ , the entrainment was strong regardless of the spacing between levels determined by  $\omega$  (reflecting, therefore, the parameter settings rather than an interaction). With increasing  $k$ , the range of  $\omega$  associated with high values of  $\tilde{r}$  became progressively narrower, reflecting the fact that, for low values of  $\omega$ , the coupling was sufficient to “pull away” the system from  $n : m$  ratio toward 1 : 1 ratio, that is, toward actual synchronization. In other words, the distributions of these parameters indicated that, under sufficiently strong coupling, the dynamics underwent a transition from being related at the ratio determined by the  $\omega$  coefficients, namely as a consequence of the choice of characteristic frequencies, toward being actually synchronized at unity ratio phase locking, especially for small values of  $\omega$ , owing to the energy exchange through the couplings. While not exactly overlapping, the region of most evident multifractality was located in the vicinity of this transition, i.e., with  $r \approx 0.3$  and  $\tilde{r} < 0.5$ . It, therefore, appears plausible that a kind of “competition” between two states at different frequency ratios gave rise to turbulence-like phenomena, opening the way to multifractality [33,34]. Confirming and elucidating the significance of this possible association is left for future work.

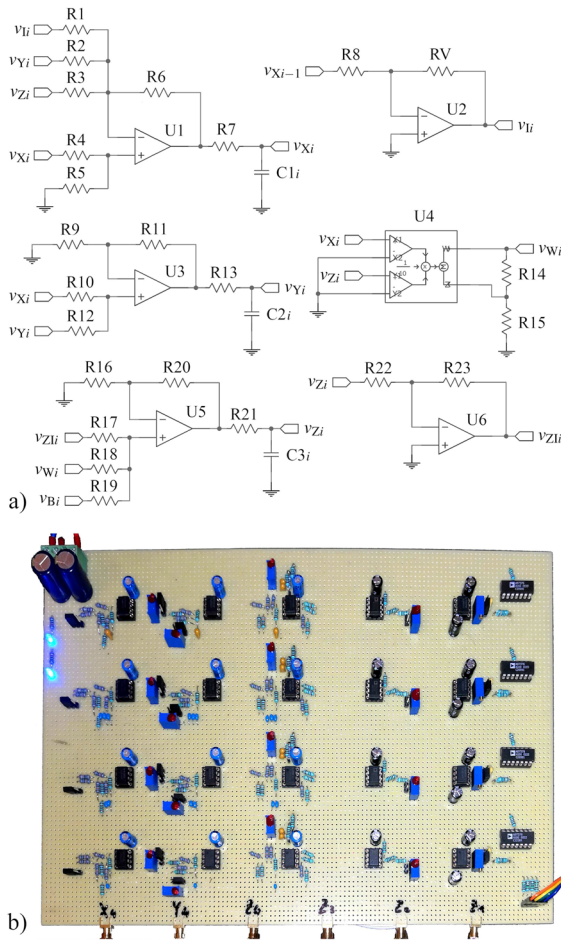


**Fig. 12** Experimental realization of the cascaded systems. **a** Circuit diagram, **b** View of the breadboard

### 4 Experiments

To confirm the generation of multifractal dynamics in a physical scenario, the cascaded Rössler systems were built in the form of analog electronic circuits based on operational amplifiers and analog multipliers. These physical circuits are not only inherently continuous, but they are also affected by parametric heterogeneities and non-ideal behaviors stemming, for instance, from component tolerances as well as further poles, zeros and offsets in the amplifiers. Therefore, they are suitable for realizing an apparatus confirming the physical observability of multifractality. Here, the differential equations were translated into circuits by associating the system variables with voltages across three capacitors to ground, and realizing the algebraic operations

via resistive networks at the inputs of the operational amplifiers [52,55]. Other possible schemes involve, for instance, configuring the amplifiers themselves as integrators [71]. The resulting circuit corresponding to each of the four cascaded systems included in Eq. (8) is shown in Fig. 12a.

In order to avoid saturation due to the limited available voltage swing, the system variables were rescaled by a factor of  $R_{20}/R_{18} = 5$ , namely, into  $v_{Xi} = x_i/5$  V,  $v_{Yi} = y_i/5$  V, and  $v_{Zi} = z_i/5$  V, as applied across the capacitors  $C_{1i}$ ,  $C_{2i}$  and  $C_{3i}$ , respectively. The equations corresponding to each of the four cascaded systems in Eq. (8) and the amplifiers U1, U3 and U5 are given by

$$\begin{cases} \frac{dv_{Xi}}{dt} = \frac{-\frac{R_6}{R_2}v_{Yi} - \frac{R_6}{R_3}v_{Zi} - \frac{R_6}{R_1}v_{li} + \left(\frac{R_6}{R_4} - 1\right)v_{Xi}}{C_{1i}R_7} \\ \frac{dv_{Yi}}{dt} = \frac{\frac{R_{11}}{R_{10}}v_{Xi} + \left(\frac{R_{11}}{R_{12}} - 1\right)v_{Yi}}{C_{2i}R_{13}}, \\ \frac{dv_{Zi}}{dt} = \frac{\frac{R_{20}}{R_{19}}v_{Bi} + \frac{R_{20}}{R_{18}}v_{Wi} + \frac{R_{20}}{R_{17}}v_{Zli} - v_{Zi}}{C_{3i}R_{21}} \end{cases} \quad (14)$$

where  $i = 1, 2 \dots 4$  and, for  $i > 1$ , U2 provides  $v_{li} = -R_V/R_8 v_{Xi-1}$ , and, for  $i = 1$ ,  $v_{li} = 0$  V. Furthermore, U4 generates  $v_{Wi} = (R_{14} + R_{15}) / (10R_{14}) v_{Xi}v_{Zi}$ , U6 provides  $v_{Zli} = -R_{23}/R_{22}v_{Zi}$ , and the control parameters are given by  $a = R_{11}/R_9 - 1$ , with  $R_9 = R_{12}$ ,  $b = R_{20}/R_{19}v_B/V$ , and  $c = R_{23}/R_{22} + 1$ . It is worth underlining that the values of  $R_5$  and  $R_{16}$  do not appear explicitly in Eq. (14) as they are uniquely determined, through circuit laws, by the other resistors.

Assuming a base resistance value of 100 kΩ, we set  $R_1 = R_2 = R_3 = R_4 = R_6 = 100$  kΩ for the  $x$ -variable adder. Consequently, one would have  $R_5 = 33$  kΩ, and only in this case the schematic in Fig. 12a corresponds to Eq. (14). However, this value had to be empirically adjusted to 40 kΩ to ensure sustained oscillation; while introducing a deviation from the algebraic relations in an ideal case, such adjustments are often necessary when realizing the Rössler system as an analog circuit, especially in the presence of external driving signals [52,72]. Similarly, for the  $y$ -variable adder, we set  $R_{10} = R_{11} = 100$  kΩ and  $R_9 = R_{12} = 87$  kΩ to obtain  $a = 0.15$ . For the  $z$ -variable adder, we set  $R_{17} = R_{19} = R_{20} = 100$  kΩ,  $R_{18} = 20$  kΩ, and  $R_{16} = 16.5$  kΩ, alongside  $R_{14} = 1$  kΩ and  $R_{15} = 9$  kΩ for multiplier scaling. Instead of applying the canonical value of 40 mV, the voltage

$v_B$  was empirically adjusted for each system to compensate the amplifier offsets and align the effect of the bifurcation parameter  $a$  to the theoretical expectation; this yielded  $v_{Bi} = \{133, 100, 90, 95\}$  mV. To realize diversified coupling strengths, we set  $R_8 = 50$  k $\Omega$  and swept  $R_V \in [0, 100]$  k $\Omega$ . Throughout the experiment, a fixed setting  $\omega = 2.5$  was adopted. We set  $R_7 = R_{13} = R_{21} = 1$  k $\Omega$ . The capacitor values were set to  $C_{u1} = 2.2$   $\mu$ F,  $C_{u2} = 880$  nF,  $C_{u3} = 350$  nF, and  $C_{u4} = 68$  nF, for  $u = \{1, 2, 3\}$ , yielding corresponding frequencies  $f_1 = 72$  Hz,  $f_2 = 181$  Hz,  $f_3 = 455$  Hz, and  $f_4 = 2341$  Hz, thus implementing  $f_2/f_1 = 2.5$ ,  $(f_3/f_1)^{1/2} = 2.51$ , and  $(f_4/f_1)^{1/4} = 2.38$ .

As shown in Fig. 12b, the circuit was assembled on a breadboard, using operational amplifiers type TL082 or equivalent, four-quadrant analog multipliers type AD633 or equivalent and digital potentiometers type AD7376A100 or equivalent. The latter were controlled via an SPI connection, and the dual power supply voltage was provided as  $\pm 15$  V. The waveforms were digitized at 16-bit, 1.25 MSA/s (aggregate over 3 or 4 channels). The signal-to-noise ratio was on the order of 100, or better. The experimental time series data have been made freely available from Ref. [73]. In brief, the recorded dynamics had qualitative features closely resembling the numerical simulations, albeit with some differences stemming from non-ideality of the physical apparatus. In particular, the volatility increased less markedly along the chain, plausibly due to the empirical adjustments described above alongside the finite supply voltage restricting the span of values accessible by the  $z_i$  variables. As the focus of this paper is on the multifractal features, for brevity these differences are not discussed in detail.

In Fig. 13, the sample fluctuation functions  $F_q(s)$  and associated multifractal spectra  $f(\alpha)$  obtained for the signals generated with two values of coupling parameter, namely  $k = 1.04$  and  $k = 0.72$ , are depicted. In the former case, shown in Fig. 13a, the fluctuation functions revealed scaling dependent on the  $q$ -moment, hallmarking multifractality. The multifractal spectrum appeared wide, with  $\Delta\alpha = 0.45$ , the maximum being located at  $\alpha_{\max} = 0.48$ , alongside an asymmetry  $A_\alpha = 0.3$  indicating a slightly more complex organization of the larger fluctuations compared to the smaller ones. On the contrary, the fractal characteristics estimated for  $k = 0.72$  confirmed the monofractal character of the analyzed signal. The fluctuation functions  $F_q(s)$  in Fig. 13b were, accordingly, essentially

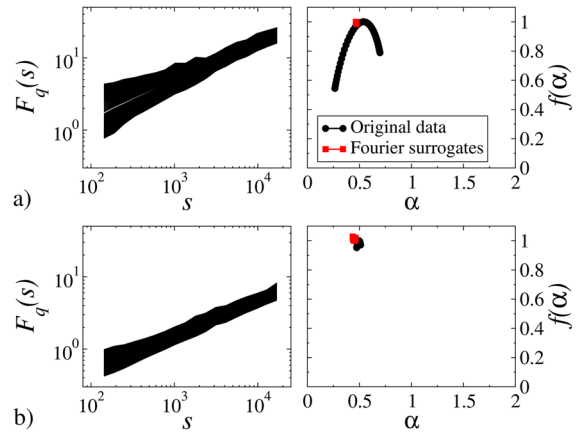


**Fig. 13** Sample fluctuation functions  $F_q(s)$  and multifractal spectrum  $f(\alpha)$  obtained for the signals from the experimental realization of the cascaded system with  $\omega = 2.5$  and **a**  $k = 1.04$  (corresponding to multifractality), and **b**  $k = 0.72$  (corresponding to monofractality)

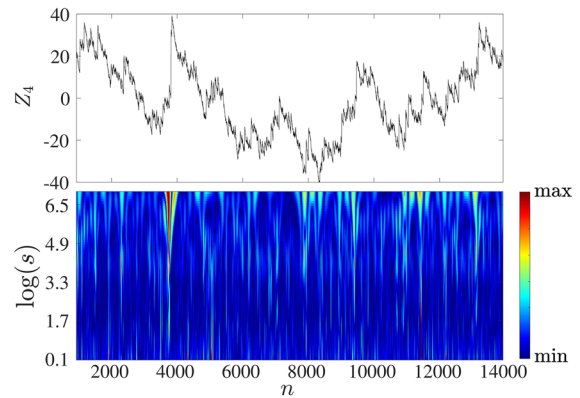


**Fig. 14** Wavelet transform of the  $z_4$  variable signal, recorded from the experimental realization, for  $\omega = 2.5$  and  $k = 1.04$  (corresponding to multifractality)

parallel, and the shape of the multifractal spectrum was close to a point, hallmarking monofractality. As previously observed for the numerical simulations, the spectra obtained for the Fourier surrogates collapsed down to a point in both cases. Furthermore, as depicted in Fig. 14, in the presence of multifractality, the cumulative sum series featured an appreciable level of volatility and the wavelet coefficients developed a tree-like organization resembling the simulation results.

The results of a systematic analysis of the experimental system concerning the coupling parameter  $k$  are depicted in Fig. 15; it should be noted that, due to the design of the physical apparatus, the bifurcation param-

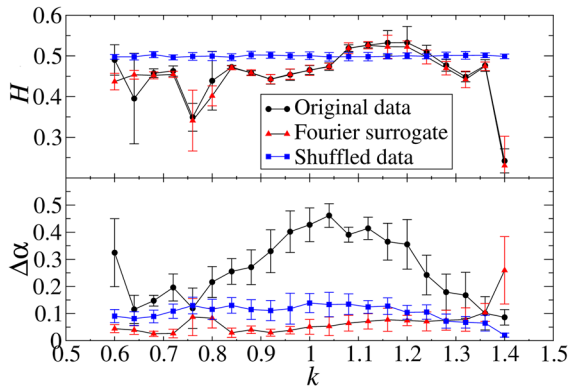


**Fig. 15** Hurst exponent and width of the multifractal spectrum estimated for the  $z_4$  variable recorded from the experimental realization of the cascaded Rössler system given different settings of the bifurcation parameter  $k$

eter was kept fixed at  $a = 0.15$  for the experiments, and the values of  $k$  had to be increased, plausibly due to the synchronization-hindering effect of non-idealities and mismatches. For most of the signals, the Hurst exponent assumed a value close to 0.5, indicating weak or absent linear dependencies. However, the width of the multifractal spectrum changed systematically as a function of the coupling strength  $k$ . The most developed multifractality, with  $\Delta\alpha \approx 0.45$ , was observed for  $k = 1.04$ , and accompanied by a gradual decay into monofractality away from this setting in both directions. Using both the Fourier and reshuffled surrogates, the spectra width shrank drastically, reassuring about the validity of the identified multifractality.

In order to more deeply investigate the multifractal character of the signals, the properties of the self-similar cascade-like model delivering the analyzed data can be analyzed. In particular, the multiplier distribution called intrinsic probability density can be recovered and examined [74]. To assess the multiplier distribution, the following procedure was applied [75, 76]. In brief, the time series of the absolute values were divided into mother boxes of uniform size, and the measure within the box was estimated as a sum of the values. Then, each of these boxes was divided into sub-boxes (daughters) of size  $l$ , and corresponding measures were calculated. The multiplier was estimated as the ratio of the daughter to mother measure. By iterative repetition of the procedure with constant  $l$  going from large to small boxes, one can obtain the skeleton of the underlying cascade with assumed  $l$  ( $l = 2$  in our case) produc-

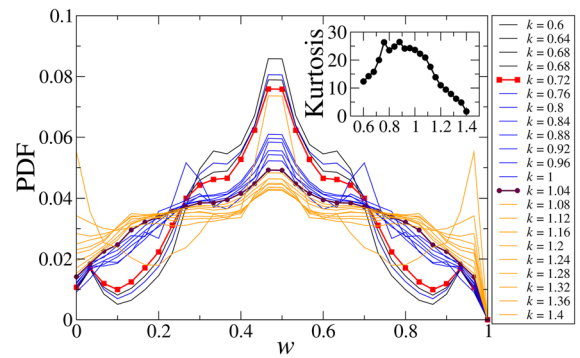


**Fig. 16** Distribution of the cascade multipliers  $w$  reconstructed for the  $z_4$  variable recorded from the experimental realization of the cascaded Rössler systems given different settings of the coupling strength  $k$

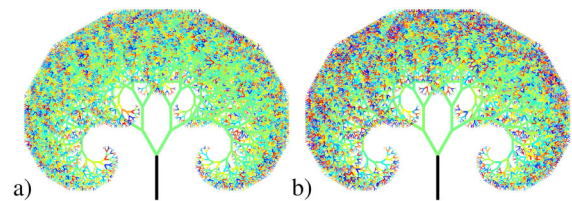


**Fig. 17** Visualization of the cascade structure reconstructed for the time series of the  $z_4$  variable recorded from the experimental realization of the cascaded Rössler systems, a) in the presence of monofractality ( $k = 0.72$ ), and b) in the presence of multifractality ( $k = 1.04$ ). See Fig. 14 for the color scale

ing the time series. The distribution of the multipliers is heterogeneous for multifractals, whereas monofractality is characterized by homogeneous multipliers.

Here, we retrieved the cascade structures and multipliers distribution for each analyzed signal according to above-described procedure. The distributions of the multipliers  $w$  for the time series depending on the  $k$  parameter are depicted in Fig. 16. It is well evident that the broadest distributions and highest kurtosis were related to signals with well-developed multifractality, whereas monofractals were associated to smaller values of kurtosis and more uniform multiplier distribution. The degree of cascade heterogeneity for monofractal and multifractal structures can also be conveniently visualized by means of Pythagoras' tree, which provides an immediate way to represent their inter-relationships. As shown in Fig. 17, wherein the values of the multipliers are coded by means of the color scale, there was considerably stronger variation of the self-similarity skeleton of the cascade for the multifractal compared to the monofractal case.

## 5 Discussion

### 5.1 Multifractal time series from deterministic chaos

According to the authors' knowledge, this work provides the first evidence of multifractal time series being generated by a fully deterministic dynamical system. In the numerical simulations, the dynamics were deterministic by construction, whereas, in the experiments, the signal-to-noise ratio was sufficiently high as to render the influence of noise negligible. There appeared to be several requirements, which we posit may be generalizable beyond the specific case of the Rössler system considered here. First, the presence of a multitude of instances of the system, diversified so as to cover a sufficient range of time scales. Second, the presence of a suitable mechanism allowing them to interact, specifically, causing the slower instances to transfer a disturbance to the faster ones. Third, operation close to the transition to chaos at an intermediate coupling strength in the vicinity of the transition between oscillation maintaining the individual system frequencies and unitary-ratio synchronization. Fourth, observation of the time series from the fastest system, through the variable where the nonlinearity acts, taking snapshots, for example via the maxima, to obtain a map-like representation.

The contribution of this paper is showing that multifractal time series can arise in such a scenario, which is fundamentally different from both random multiplicative processes, that involve an extrinsic source of turbulence, and abstract mathematical constructs such as the binomial cascade and iterated maps, which are more removed from the nonlinear dynamics of physical, biological and other systems. In a previous paper, it was shown that artefactual multifractal-like signatures could emerge in the dynamics of chaotic systems such as the Saito circuit [16]. By contrast, here, an extended set of analyses confirmed the true and fully developed multifractality of the signals. Representative results revealed an almost perfect scaling with a broad and symmetric multifractal spectrum similar to the one identified for the binomial cascade. Moreover, bidimensional parametric sweeps highlighted a sort of multifractal path along an edge between two extreme system behaviors, corresponding to different dynamical states. On the other hand, there appeared to be no immediate correspondence with the Lyapunov spectrum. Numerical simulations of the processes related

to the observed variable based on the cascade approach and analysis of the recovered cascade parameters confirmed the statistical similarity to the well-established multifractal cascades. At the same time, experimental realization confirmed that the approach is immediately viable to obtain a physical apparatus. The corresponding electronic circuit is arguably more complex than the one previously proposed based on the random multiplicative approach but, crucially, its operation is not based on the presence of a noise source; in other words, here, multifractality was a intrinsic product of the dynamics as opposed to a consequence of a non-trivial manipulation of externally supplied entropy [39,40].

### 5.2 Time series vs. attractor geometry

The relationship between multifractality and turbulent dynamics has been investigated extensively, and so has the multifractal organization of attractor geometries and iterated maps [33,77]. The gap that this work intended to plug specifically pertains to the properties and the generation of multifractal time series, commonly observed using the detrended fluctuation analysis and wavelet decomposition [15]. This is distinct from early methods based on the reconstruction of attractor geometry, which are ill-suited for analyzing the time series generated by large-scale complex systems, such as financial, social and biological ones, due to the issues in finding suitable embeddings because of their inherently high-dimensional nature [12,78,79]. For example, the  $f(\alpha)$  formalism was applied to study the attractor geometries generated by a relaxation oscillator based on an operational amplifier and driven by an external signal, by diode-resonator systems as well as by mercury convection apparatuses [41,80–82]. Those observations, notably, predate by several years the introduction of the MF DFA and the usage of wavelets to investigate multifractality as is commonplace today,  $f(\alpha)$  measured the dimension of the set of singularities on the attractor, which is not equivalent to the present time series analyses [15,83].

In fact, our results motivate further research attempting to clarify the precise relationship between multifractality observed on time series, as prevalently applied nowadays to study large-scale complex systems, and multifractality observed on attractor geometry, as extensively investigated in earlier works on more

elementary, small-scale physical apparatuses. Such an effort, which goes well beyond the scope of the present work, should include systematically reanalyzing the results of those experiments using current methods such as MF DFA. One aspect of similarity with this literature is that, as previously observed for diode-resonator circuits and other systems, also in the present case multifractality tended to arise preferentially for control parameter settings close to the onset of chaos, namely, within the period-doubling cascade characterizing the Rössler system [41,81,82]. Another previously established observation is that of the transfer of multifractality from more turbulent to more regular systems, which recalls the cascade structure of the present arrangement and the fact that multifractality was increasingly evident along the chain [33]. Future work should explore the generality of our findings in the context of other chaotic systems having different qualitative properties such as double- and multi-scroll attractors, as well as in more elementary electronic circuits including single transistor-based chaotic oscillators [24,25]. It is worth underlining further that, even though the multifractal analysis was performed on the series of maxima, primarily to attenuate the effect of autocorrelation, the underlying dynamics are continuous, therefore, fundamentally different from iterated maps. Another aspect of interest that remains unexplored is the potential relationship between the topology of the structural connections and the emergence of multifractality in more complex networks [84].

### 5.3 Future work

One motivation for the present work was related to the ongoing efforts to create numerical systems and physical apparatuses as simple as possible that can capture key statistical properties of neural dynamics across scales, to be used both in the construction of “toy models” of biological brains and toward the advancement of physical reservoir computing [29]. While diverse mechanisms of pattern formation via synchronization and the relationship between connectivity and dynamics have been successfully captured, multifractality remained somewhat elusive. This represented an important shortcoming, considering that multifractality is a fundamental statistical signature of physiological function across signals as diverse as the electrocardiogram, electroencephalogram, brain hemodynamic

and autonomic recordings; accordingly, a variety of means have been proposed to estimate the singularity spectrum from such signals and investigate its alteration in pathological states [5,6,85–89]. Taking the apparatus introduced here as a model of multifractality as observed at the meso- and macroscopic scales in physiological systems, future work will investigate the network-level phenomena that can arise when multiple systems are made to interact. It appears plausible that this model will be both richer and more plausible compared to the low-dimensional chaotic circuits, generating monofractal dynamics, that have been proposed thus far.

**Acknowledgements** LM gratefully acknowledges the support of the “Hundred Talents” program of the University of Electronic Science and Technology of China. All experimental activities were self-funded and conducted by LM during the period 2020–2021 using own independent assets located in Grigno TN, Italy; the manuscript was later finalized after joining the University of Electronic Science and Technology of China, to which no equipment was transferred. The authors are grateful to anonymous reviewers for constructive suggestions.

**Author contributions** All authors contributed to the study conception and design. Material preparation and data collection were performed by LM. Data analysis was performed by PO and LM. The first draft was written in equal measures by PO and LM and all authors commented on previous versions of the manuscript. All authors read and approved the final text.

**Funding** This work has been supported by a grant from the Priority Research Area DigiWorld under the Strategic Programme Excellence Initiative of the Jagiellonian University, as well as by the Chengdu Science and Technology Bureau Program under Grant 2022GH02-00042-HZ and the CNS program of UESTC No. Y0301902610100201. This research has also been supported by the Foundation for Polish Science co-financed by the European Union under the European Regional Development Fund in the POIR.04.04.00-00-14DE/18-00 project carried out within the Team-Net program.

**Data Availability** The experimental datasets generated during the current study are available at <http://dx.doi.org/10.5281/zenodo.8260933>.

**Conflict of interest** The authors have no relevant financial or non-financial interests to disclose.

## References

1. Pietronero, L., Tosatti, E.: *Fractals in Physics*. North Holland, (012)
2. Subramaniam, A.R., Gruzberg, I.A., Ludwig, A.W.W.: Boundary criticality and multifractality at the two-

- dimensional spin quantum hall transition. *Phys. Rev. B* **78**, 245105 (2008)
3. Klamut, J., Kutner, R., Gubiec, T., Struzik, Z.R.: Multi-branch multifractality and the phase transitions in time series of mean interevent times. *Phys. Rev. E* **101**, 063303 (2020)
  4. Stanley, H.E., Meakin, P.: Multifractal phenomena in physics and chemistry. *Nature* **335**, 405–409 (1998)
  5. Franca, L.G.S., Miranda, J.G.V., Leite, M., Sharma, N.K., Walker, M.C., Lemieux, L., Wang, Y.: Fractal and multifractal properties of electrographic recordings of human brain activity: toward its use as a signal feature for machine learning in clinical applications. *Front. Physiol.* **9**, 1767 (2018)
  6. Ochab, J.K., Watorek, M., Ceglarek, A., Fafrowicz, M., Lewandowska, K., Marek, T., Sikora-Wachowicz, B., Oświęcimka, P.: Task-dependent fractal patterns of information processing in working memory. *Sci. Rep.* **12**, 17866 (2022)
  7. Gao, X.L., Shao, Y.H., Yang, Y.H., Zhou, W.X.: Do the global grain spot markets exhibit multifractal nature? *Chaos Soliton Fractals* **164**, 112663 (2022)
  8. Oświęcimka, P., Kwapien, J., Drożdż, S.: Multifractality in the stock market: price increments versus waiting times. *Phys. A* **347**, 626–638 (2005)
  9. Buonocore, R.J., Aste, T., Di Matteo, T.: Measuring Multiscaling in financial time-series. *Chaos Solitons Fractals* **88**, 38–47 (2016)
  10. Drożdż, S., Oświęcimka, P., Kulig, A., Kwapien, J., Bazarnik, K., Grabska-Gradzińska, I., Rybicki, J., Stanuszek, M.: Quantifying origin and character of long-range correlations in narrative texts. *Inf. Sci.* **331**, 32–44 (2016)
  11. Jafari, G.R., Pedram, P., Hedayatifar, L.: Long-range correlation and multifractality in Bach's inventions pitches. *J. Stat. Mech Theory Exp.* **2007**, P04012 (2007)
  12. Leis, V., Radke, B., Gubichev, A., Mirchev, A., Boncz, P., Kemper, A., Neumann, T.: Fractal measures and their singularities: the characterization of strange sets. *Phys. Rev. A* **33**, 1141–1151 (1986)
  13. Kwapien, J., Drożdż, S.: Physical approach to complex systems. *Phys. Rep.* **515**, 115 (2012)
  14. Muzy, J.F., Bacry, E., Arneodo, A.: The multifractal formalism revisited with wavelets. *Int. J. Bifurcat. Chaos* **4**, 245–302 (1994)
  15. Kantelhardt, J.W., Zschiegner, S.A., Koscielny-Bunde, E., Havlin, S., Bunde, A., Stanley, H.E.: Multifractal detrended fluctuation analysis of nonstationary time series. *Phys. A* **316**(1), 87–114 (2002)
  16. Oświęcimka, P., Drożdż, S., Frasca, M., Gębarowski, R., Yoshimura, N., Zunino, L., Minati, L.: Wavelet-based discrimination of isolated singularities masquerading as multifractals in detrended fluctuation analyses. *Nonlinear Dyn.* **100**(2), 1689–1704 (2020)
  17. Oświęcimka, P., Drożdż, S., Forczek, M., Jadach, S., Kwapien, J.: Detrended cross-correlation analysis consistently extended to multifractality. *Phys. Rev. E* **89**, 023305 (2014)
  18. Meneveau, C., Sreenivasan, K.R.: The multifractal nature of turbulent energy dissipation. *J. Fluid Mech.* **224**, 429–484 (1991)
  19. Mandelbrot, B., Fisher, A., Calvet, L.: A multifractal model of asset returns. *Foundation Discussion Paper*, p. 1164 (1997)
  20. Bacry, E., Delour, J., Muzy, J.F.: Multifractal random walk. *Phys. Rev. E* **64**, 026103 (2001)
  21. Boccaletti, S., Kurths, J., Osipov, G., Valladares, D.L., Zhou, C.S.: The synchronization of chaotic systems. *Phys. Rep.* **366**(1), 1–101 (2002)
  22. Lundberg, K.H.: The history of analog computing: introduction to the special section. *IEEE Control. Syst.* **25**(3), 22–25 (2005)
  23. Minati, L., Mancinelli, M., Frasca, M., Bettotti, P., Pavesi, L.: An analog electronic emulator of non-linear dynamics in optical microring resonators. *Chaos Solitons Fractals* **153**, 111410 (2021)
  24. Chen, G., Ueta, T.: *Chaos in circuits and systems*. World Scientific (2002)
  25. Sprott, J.C., Thio, W.J.-C.: *Elegant circuits*. World Scientific (2022)
  26. Zangeneh-Nejad, F., Sounas, D.L., Alù, A., Fleury, R.: Analogue computing with metamaterials. *Nat. Rev. Mater.* **6**(3), 207–225 (2021)
  27. Tanaka, G., Yamane, T., Héroux, J.B., Nakane, R., Kanazawa, N., Takeda, S., Numata, H., Nakano, D., Hirose, A.: Recent advances in physical reservoir computing: a review. *Neural Netw.* **115**, 100–123 (2019)
  28. Glazier, J.A., Libchaber, A.: Quasi-periodicity and dynamical systems: an experimentalist's view. *IEEE Trans. Circuits Syst.* **35**(7), 790–809 (1988)
  29. Minati, L.: Across neurons and silicon: some experiments regarding the pervasiveness of nonlinear phenomena. *Acta Phys. Pol. B* **49**, 2029 (2018)
  30. Riedi, R.H., Crouse, M.S., Ribeiro, V.J., Baraniuk, R.G.: A multifractal wavelet model with application to network traffic. *IEEE Trans. Inf. Theory* **45**(3), 992–1018 (1999)
  31. Li, J., Ma, X., Zhao, M., Cheng, X.: A novel MFDDFA algorithm and its application to analysis of harmonic multifractal features. *Electronics* **8**(2), 209 (2019)
  32. Qiang, W., Cao, H.: Multifractal behavior of the power dissipation of cmos circuits. In: 2008 IEEE International Conference on Electron Devices and Solid-State Circuits, pp. 1–4 (2008)
  33. Mahmoodi, K., West, B.J., Grigolini, P.: On the dynamical foundation of multifractality. *Phys. A* **551**, 124038 (2020)
  34. Benzi, R., Paladin, G., Parisi, G., Vulpiani, A.: On the multifractal nature of fully developed turbulence and chaotic systems. *J. Phys. A* **17**(18), 3521 (1984)
  35. Luo, A.C.J.: *Chaos and Multifractality*, pp. 137–167. Springer, New York (2012)
  36. Volpe, G., Wehr, J.: Effective drifts in dynamical systems with multiplicative noise: a review of recent progress. *Rep. Prog. Phys.* **79**(5), 053901 (2016)
  37. Redner, S.: Random multiplicative processes: an elementary tutorial. *Am. J. Phys.* **58**(3), 267–273 (1990)
  38. da Silva, M.P., Lya, M.L., Jr., Vermelho, M.V.D.: Analog study of the first passage time problem driven by power-law distributed noise. *Physica A* **348**, 85–96 (2005)
  39. Sato, A.-H., Takayasu, H., Sawada, Y.: Power law fluctuation generator based on analog electrical circuit. *Fractals* **08**(03), 219–225 (2000)

40. Silva, L.B.M., Vermelho, M.V.D., Lyra, M.L., Viswanathan, G.M.: Multifractal detrended fluctuation analysis of analog random multiplicative processes. *Chaos, Solitons Fractals* **41**(5), 2806–2811 (2009)
41. Su, Z., Rollins, R.W., Hunt, E.R.: Measurements of  $f(\alpha)$  spectra of attractors at transitions to chaos in driven diode resonator systems. *Phys. Rev. A* **36**, 3515–3517 (1987)
42. Müller, S., Heusler, S., Braun, P., Haake, F., Altland, A.: Periodic-orbit theory of universality in quantum chaos. *Phys. Rev. E* **72**, 046207 (2005)
43. Sgrignuoli, F., Gorsky, S., Britton, W.A., Zhang, R., Riboli, F., Dal Negro, L.: Multifractality of light in photonic arrays based on algebraic number theory. *Nat. Commun. Phys.* **3**(1), 106 (2020)
44. Napoli, E., D’Arco, M., Genovese, M., Schiano Lo, R.: A complete system to generate electrical noise with arbitrary power spectral density. *Measurement* **72**, 9–19 (2015)
45. Wang, F., Li, Z.-S., Liao, G.-P.: Multifractal detrended fluctuation analysis for image texture feature representation. *Int. J. Pattern Recognit Artif Intell.* **28**, 1455005 (2014)
46. Oświęcimka, P., Livi, L., Drożdż, S.: Right-side-stretched multifractal spectra indicate small-worldness in networks. *Commun. Nonlinear Sci. Numer. Simul.* **57**, 231–245 (2018)
47. Oświęcimka, Paweł, Minati, Ludovico: *5 Multifractal characteristics of singular signals*, pages 99–112. De Gruyter, Berlin, Boston (2022)
48. Drożdż, S., Oświęcimka, P.: Detecting and interpreting distortions in hierarchical organization of complex time-series. *Phys. Rev. E* **91**, 030902(R) (2015)
49. Schreiber, T., Schmitz, A.: Surrogate time series. *Physica D* **142**(3), 346–382 (2000)
50. Barrio, R., Blesa, F., Serrano, S.: Qualitative analysis of the rössler equations: bifurcations of limit cycles and chaotic attractors. *Physica D* **238**(13), 1087–1100 (2009)
51. Maris, D.T., Goussis, D.A.: The “hidden” dynamics of the rössler attractor. *Physica D* **295–296**, 66–90 (2015)
52. Minati, L., Li, C., Bartels, J., Chakraborty, P., Li, Z., Yoshimura, N., Frasca, M., Ito, H.: Accelerometer time series augmentation through externally driving a non-linear dynamical system. *Chaos, Solitons Fractals* **168**, 113100 (2023)
53. Rössler, O.E.: Chaotic behavior in simple reaction system. *Zeitschrift für Naturforschung A* **31**, 259–264 (1976)
54. Rössler, O.E.: An equation for continuous chaos. *Phys. Lett. A* **57**(5), 397–398 (1976)
55. Buscarino, A., Fortuna, L., Frasca, M., Sciuto, G.: *A Concise Guide to Chaotic Electronic Circuits*. Springer, Cham, Switzerland (2014)
56. Minati, L., Frasca, M., Giustolisi, G., Oświęcimka, P., Drożdż, S., Ricci, L.: High-dimensional dynamics in a single-transistor oscillator containing Feynman-Sierpiński resonators: effect of fractal depth and irregularity. *Chaos* **28**(9), 093112 (2018)
57. Zhou, Y., Hua, Z., Pun, C.-M., Philip, C.L.: Cascade chaotic system with applications. *IEEE Trans. Cybern.* **45**(9), 2001–2012 (2015)
58. de Godoy, Stênio, J.W., Ling, L.L.: Modern network traffic modeling based on binomial multiplicative cascades. *J. Supercomput.* **71**(5), 1712–1735 (2015)
59. Heurteaux, Y.: *An Introduction to Mandelbrot Cascades*, pp. 67–105. Springer, Cham (2016)
60. Ott, E.: *Chaos in Dynamical Systems*, 2nd edn. Cambridge University Press, Cambridge (2002)
61. Huang, L., Chen, Q., Lai, Y.-C., Pecora, L.M.: Generic behavior of master-stability functions in coupled nonlinear dynamical systems. *Phys. Rev. E* **80**, 036204 (2009)
62. Buscarino, A., Frasca, M., Branciforte, M., Fortuna, L., Sprott, J.C.: Synchronization of two rössler systems with switching coupling. *Nonlinear Dyn.* **88**(1), 673–683 (2017)
63. Atkinson, K.E., Han, W., Stewart, D.: *Taylor and Runge-Kutta methods*, pp. 67–93. Wiley, Hoboken (2009)
64. Oświęcimka, P., Drożdż, S., Kwapien, J., Górski, A.Z.: Effect of detrending on multifractal characteristics. *Acta Phys. Pol.* **123**, 597–603 (2013)
65. Kantz, H., Schreiber, T.: *Nonlinear Time Series Analysis*, 2nd edn. Cambridge University Press, Cambridge (2003)
66. Benettin, G., Galgani, L., Giorgilli, A., Strelcyn, J.M.: Lyapunov characteristic exponents for smooth dynamical systems and for Hamiltonian systems; a method for computing all of them. Part 1: Theory. *Meccanica* **15**, 9–20 (1980)
67. Benettin, G., Galgani, L., Giorgilli, A., Strelcyn, J.M.: Lyapunov characteristic exponents for smooth dynamical systems and for Hamiltonian systems; a method for computing all of them. Part 2: numerical application. *Meccanica* **15**, 21–30 (1980)
68. Boashash, B.: Estimating and interpreting the instantaneous frequency of a signal. ii. Algorithms and applications. *Proc. IEEE* **80**(4), 540–568 (1992)
69. Reilly, A., Frazer, G., Boashash, B.: Analytic signal generation-tips and traps. *IEEE Trans. Signal Process.* **42**(11), 3241–3245 (1994)
70. Ermentrout, G.B.: n:m phase-locking of weakly coupled oscillators. *J. Math. Biol.* **12**(3), 327–342 (1981)
71. Ibrahim, K.M., Jamal, R.K., Ali, F.H.: Chaotic behaviour of the rössler model and its analysis by using bifurcations of limit cycles and chaotic attractors. *J. Phys: Conf. Ser.* **1003**(1), 012099 (2018)
72. Minati, L., Frasca, M., Valdes-Sosa, P.A., Barbot, J.-P., Letellier, C.: Flatness-based real-time control of experimental analog chaotic oscillators. *Chaos, Solitons Fractals* **177**, 114274 (2023)
73. Additional time series recorded from the analog circuit downloadable from, 2023. <http://dx.doi.org/10.5281/zenodo.8260933>
74. Chhabra, A.B., Sreenivasan, K.R.: Scale-invariant multiplier distributions in turbulence. *Phys. Rev. Lett.* **68**, 2762 (1992)
75. Sreenivasan, K.R., Stolovitzky, G.: Turbulent cascades. *J Stat. Phys.* **78**, 311 (1995)
76. Jiango, Z.-Q., Zhou, W.-X.: Scale invariant distribution and multifractality of volatility multipliers in stock markets. *Phys. A* **381**, 343–350 (2007)
77. McCauley, J.L.: Introduction to multifractals in dynamical systems theory and fully developed fluid turbulence. *Phys. Rep.* **189**(5), 225–266 (1990)
78. Jensen, M.H., Kadanoff, L.P., Libchaber, A., Procaccia, I., Stavans, J.: Global universality at the onset of chaos: Results of a forced rayleigh-bénard experiment. *Phys. Rev. Lett.* **55**, 2798–2801 (1985)
79. Perinelli, A., Ricci, L.: Identification of suitable embedding dimensions and lags for time series generated by chaotic, finite-dimensional systems. *Phys. Rev. E* **98**, 052226 (2018)

80. Barkley, D., Cumming, A.: Thermodynamics of the quasiperiodic parameter set at the borderline of chaos: experimental results. *Phys. Rev. Lett.* **64**, 327–331 (1990)
81. Glazier, J.A., Gunaratne, G., Libchaber, A.:  $f(\alpha)$  curves: experimental results. *Phys. Rev. A* **37**, 523–530 (1988)
82. Su, Z., Rollins, R.W., Hunt, E.R.: Universal properties at the onset of chaos in diode resonator systems. *Phys. Rev. A* **40**, 2689–2697 (1989)
83. Arneodo, A., Bacry, E., Muzy, J.F.: The thermodynamics of fractals revisited with wavelets. *Physica A*, 213(1):232–275, Proceedings of the Third European Days of Thermodynamics on Inhomogeneous Phases and Pattern Formation (1995)
84. Minati, L., Ito, H., Perinelli, A., Ricci, L., Faes, L., Yoshimura, N., Koike, Y., Frasca, M.: Connectivity influences on nonlinear dynamics in weakly-synchronized networks: insights from rössler systems, electronic chaotic oscillators, model and biological neurons. *IEEE Access* **7**, 174793–174821 (2019)
85. Racz, F.S., Stylianou, O., Mukli, P., Eke, A.: Multifractal and entropy analysis of resting-state electroencephalography reveals spatial organization in local dynamic functional connectivity. *Sci. Rep.* **9**(1), 13474 (2019)
86. Lin, D.C., Sharif, A.: Common multifractality in the heart rate variability and brain activity of healthy humans. *Chaos* **20**(2), 023121 (2010)
87. Guan, S., Wan, D., Yang, Y., Biswal, B.: Sources of multifractality of the brain rs-fMRI signal. *Chaos, Solitons Fractals* **160**, 112222 (2022)
88. Ghosh, D., Samanta, S., Chakraborty, S.: Multifractal Correlation Study Between Posture and Autonomic Deregulation Using ECG and Blood Pressure Data, pp. 149–172. Springer, Singapore (2019)
89. Ivanov, P.C., Amaral, L.A.N., Goldberger, A.L., Havlin, S., Rosenblum, M.G., Struzik, Z.R., Stanley, H.E.: Multifractality in human heartbeat dynamics. *Nature* **399**(6735), 461–465 (1999)

**Publisher's Note** Springer Nature remains neutral with regard to jurisdictional claims in published maps and institutional affiliations.

Springer Nature or its licensor (e.g. a society or other partner) holds exclusive rights to this article under a publishing agreement with the author(s) or other rightsholder(s); author self-archiving of the accepted manuscript version of this article is solely governed by the terms of such publishing agreement and applicable law.